Inorg. Chem. **2006**, *45*, 2307−2316

Mononuclear $[Ni^{II}(L)(P\text{-}(o\text{-}C_6H_4S)_2(o\text{-}C_6H_4SH))]^{0/1-}$ (L = Thiolate, Selenolate, PPh_3, and Cl) Complexes with Intramolecular [Ni···S···H···S]/[Ni···H···S] Interactions Modulated by the Coordinated Ligand L: Relevance to the [NiFe] Hydrogenases

Chien-Hong Chen,[†] Gene-Hsiang Lee,[‡] and Wen-Feng Liaw*,[†]

Department of Chemistry, National Tsing Hua University, Hsinchu 30043, Taiwan, and Instrumentation Center, National Taiwan University, Taipei, Taiwan

Received November 7, 2005

The shift of the IR ν_{S-H} frequency to lower wavenumbers for the series of complexes $[Ni^{II}(L)(P\text{-}(o\text{-}C_6H_4S)_2(o\text{-}C_6H_4\text{-}SH))]^{0/1-}$ (L = PPh_3 (**1**), Cl (**6**), Se-*p*-C_6H_4-Cl (**5**), S-C_4H_3S (**7**), SePh (**4**)) indicates that a trend of increasing electronic donation of the L ligands coordinated to the Ni(II) center promotes intramolecular [Ni–S···H–S] interactions. Compared to the Ni···S(H) distance, in the range of 3.609–3.802 Å in complexes **1** and **4**–**7**, the Ni···S(CH_3) distances of 2.540 and 2.914 Å observed in the $[Ni^{II}(PPh_3)(P(o\text{-}C_6H_4S)_2(o\text{-}C_6H_4\text{-}SCH_3))]$ complexes (**8a** and **8b**, two conformational isomers with the chemical shift of the thioether methyl group at δ 1.820 (–60 °C) and 2.109 ppm (60 °C) (C_4D_8O)) and the Ni···S(CH_3) distances of 3.258 and 3.229 Å found in the $[Ni^{II}(L)(P(o\text{-}C_6H_4S)_2(o\text{-}C_6H_4\text{-}SCH_3))]^{1-}$ complexes (L = SPh (**9**), SePh (**10**)) also support the idea that the pendant thiol protons of the Ni(II)–thiol complexes **1**/**4**–**7** were attracted by both the sulfur of thiolate and the nickel. The increased basicity (electronic density) of the nickel center regulated by the monodentate ligand attracted the proton of the pendant thiol effectively and caused the weaker S···H bond. In addition, the pendant thiol interaction modes in the solid state (complexes **1a** and **1b**, Scheme 1) may be controlled by the solvent of crystallization. Compared to complex **1a**, the stronger intramolecular [Ni–S···H–S] interaction (or a combination of [Ni–S···H–S]/[Ni···H–S] interactions) found in complexes **4**–**7** led to the weaker S–H bond strength and accelerated the oxidation (by O_2) of complexes **4**–**7** to produce the $[Ni^{Y}(L)(P(o\text{-}C_6H_4S)_3)]^{1-}$ (L = Se-*p*-C_6H_4–Cl (**11**), SePh (**12**), S-C_4H_3S (**13**)) complexes.

Introduction

Molecular hydrogen plays an important role in the metabolism of many microorganisms. Hydrogenases catalyze the reversible two-electron oxidation of H_2 in aerobic and anaerobic microorganisms.[1,2] Two classes of hydrogenases, [Fe]-only hydrogenases ([Fe]-only H_2ases) and [NiFe] hydrogenases ([NiFe] H_2ases), have been studied widely.[1,2] [Fe]-only H_2ases are usually associated with hydrogen production, and [NiFe] H_2ases are generally involved in hydrogen uptake.[3−7] The X-ray crystallographic studies of the active-site structure of [NiFe] hydrogenases isolated from *D. gigas*, *D. vulgaris*, *D. fructosovorans*, and *D. desulfuri-*

* To whom correspondence should be addressed. E-mail: wfliaw@mx.nthu.edu.tw.
† National Tsing Hua University.
‡ National Taiwan University.

(1) (a) Adams, M. W. W.; Mortenson, L. E.; Chen, J.-S. *Biochim. Biophys. Acta* **1981**, *594*, 105−176. (b) Adams, M. W. W.; Stiefel, E. I. *Curr. Opin. Chem. Biol.* **2000**, *4*, 214−220.
(2) (a) Carepo, M.; Tierney, D. L.; Brondino, C. D.; Yang, T. C.; Pamplona, A.; Telser, J.; Moura, I.; Moura, J. J. G.; Hoffman, B. M. *J. Am. Chem. Soc.* **2002**, *124*, 281−286. (b) Albracht, S. P. J. *Biochim. Biophys. Acta* **1994**, *1188*, 167−204. (c) van der Zwaan, J. W.; Coremans, J. M. C. C.; Bouwens, E. C. M.; Albracht, S. J. P. *Biochim. Biophys. Acta* **1990**, *1041*, 101−110. (d) Vignais, P. M.; Billoud, B.; Meyer, J. *FEMS Microbiol. Rev.* **2001**, *25*, 455−501.
(3) (a) Peters, J. W.; Lanzilotta, W. N.; Lemon, B. J.; Seefeldt, L. C. *Science* **1998**, *282*, 1853−1858. (b) Nicolet, Y.; Piras, C.; Legrand, P.; Hatchikian, C. E.; Fontecilla-Camps, J. C. *Structure* **1999**, *7*, 13−23. (c) Lemon, B. J.; Peters, J. W. *J. Am. Chem. Soc.* **2000**, *122*, 3793−3794. (d) Nicolet, Y.; de Lacey, A. L.; Vernéde, X.; Fernandez, V. M.; Hatchikian, E. C.; Fontecilla-Camps, J. C. *J. Am. Chem. Soc.* **2001**, *123*, 1596−1601.
(4) (a) Volbeda, A.; Charon, M. H.; Piras, C.; Hatchikian, E. C.; Frey, M.; Fontecilla-Camps, J. C. *Nature* **1995**, *373*, 580−587. (b) Garcin, E.; Vernede, X.; Hatchikian, E. C.; Volbeda, A.; Frey, M.; Fontecilla-Camps, J.-C. *Structure* **1999**, *7*, 557−566. (c) Happe, R. P.; Roseboom, W.; Pierik, A. J.; Albracht, S. P. J. *Nature* **1997**, *385*, 126. (d) Volbeda, A.; Garcin, E.; Piras, C.; De Lacey, A. L.; Fernandez, V. M.; Hatchikian, E. C.; Frey, M.; Fontecilla-Camps, J. C. *J. Am. Chem. Soc.* **1996**, *118*, 12989−12996.

10.1021/ic051924w CCC: $33.50 © 2006 American Chemical Society
Published on Web 02/07/2006

cans ATCC27774 in combination with infrared spectroscopy have revealed an active site comprised of a heterobimetallic $(S_{cys})_2Ni(\mu\text{-}S_{cys})_2(\mu\text{-}X)Fe(CO)(CN)_2$ (X = O, OH) cluster.[4−7] The bridging ligand, X, was proposed to be an oxide or hydroxide in the oxidized state and was found to be absent in the reduced state. The geometry of nickel in the active site of [NiFe] H_2ases is pseudotetrahedral in the reduced state and pseudosquare-pyramidal in the oxidized state. During the catalytic cycle of [NiFe] H_2ases, the various catalytic states corresponding to IR vibrations, the EPR *g* value, and E_m values (vs NHE) were proposed; the formal oxidation state of the nickel center in the Ni-A, Ni-B, and Ni-C states is a paramagnetic Ni(III), while it is a Ni(II) in the Ni-R, Ni-SU, Ni-SI, and Ni-SIa states.[8] Hall and De Gioia suggested that the Ni-R state existed as $[(S_{cys}\text{-}H)(S_{cys})Ni^{II}(\mu\text{-}S_{cys})_2Fe(CO)(CN)_2]$ and $[(S_{cys}\text{-}H)(S_{cys})Ni^{II}(\mu\text{-}H)(\mu\text{-}S_{cys})_2\text{-}Fe(CO)(CN)_2]$ with a Scys···H interacting directly with the nickel center (a $[Ni\cdots H\text{-}S_{cys}]$ interaction).[9,10] Both of the proposed mechanisms suggested that the intermediate Ni-C state existed as $[(S_{cys}\text{-}H)(S_{cys})Ni^{III}(\mu\text{-}H)(\mu\text{-}S_{cys})_2Fe(CO)\text{-}(CN)_2]$, a hydride bridge. Also, the architecture of the silent-active Ni-SIa is proposed to be a Cys···SH proton directly interacting with nickel, $[(S_{cys}\text{-}H)(S_{cys})Ni^{II}(\mu\text{-}S_{cys})_2Fe(CO)\text{-}(CN)_2]$. Early electron nuclear double resonance (ENDOR) studies have provided evidence for the existence of a solvent exchangeable proton which may coordinate to the Ni atom as an in-plane hydride form or as a η^2-H_2 form.[11] Recently, ENDOR and hyperfine sublevel correlation spectroscopy (HYSCORE) have been applied to study the active site of the catalytic [NiFe] hydrogenase from *D. vulgaris* Miyazaki F. in the reduced Ni-C state.[5c−d,12] These techniques have provided direct experimental evidence for the hydride bridging between the nickel and iron atoms. The Ni-C state was suggested to be either an early product of the heterolytic cleavage of H_2 or a precursor to H_2 formation.[12]

Several mononuclear nickel−thiolate complexes have been synthesized to obtain information about the structure of Ni in the active site of the [NiFe] H_2ase.[13] Complex $Ni^{II}(Bm^{Me})_2$ (Bm^{Me} = bis(2-mercapto-1-methylimidazolyl)borate) with a $[NiS_4H_2]$ core and an Ni···H−B interaction may provide a structural model of the nickel site of a [NiFe] H_2ase.[14] Model complex $[Ni^{II}(SC(NH_2)NHNCH\text{-}C_6H_4\text{-}o\text{-}OH)_2]$ with the labile phenolic OH group catalyzes the isotopic exchange of D_2 with the phenol OH proton upon exposure of a DMSO/ethanol solution of the Ni complex to D_2.[15] Recent kinetic studies of the protonation of complexes $[Ni(SPh)(triphos)]^+$, $[Ni(SePh)(triphos)]^+$, and $[Ni(SEt)(triphos)]^+$ (triphos = $(Ph_2PCH_2CH_2)_2PPh$) revealed that the sulfur atom's lone pair of electrons is the initial site for the protonation of $[Ni(SR)\text{-}(triphos)]^+$.[16] However, for the more electron-donating alkylthiolate ligand ligated to Ni, interaction of the proton with both the nickel and sulfur sites (an η^2-EtS−H complex) was proposed.[16] Recently, Tatsumi and co-workers reported the isolation of dithiolato-bridged [NiFe] complexes, $[Fe(CO)_2\text{-}(CN)_2(\mu\text{-}SCH_2CH_2CH_2S)Ni(S_2CNR_2)]^-$ (R = Et; R_2 = $-(CH_2)_5-$). These complexes display the close structural feature of the active site of reduced form [NiFe] H_2ase.[17]

In the previous study of the $[Ni^{II}(L)(P\text{-}(o\text{-}C_6H_4S)_2(o\text{-}C_6H_4\text{-}SH))]$ (L = SePh (**4**), S-C_4H_3S (**7**)) complexes, the interaction between the thiol proton and both the nickel and sulfur atoms (a combination of intramolecular [Ni−S···H−S] and [Ni···H−S] interactions) was demonstrated.[18] The desire to explore the correlation between the extent of the interactions and the basicity (electronic density) of nickel has inspired us to synthesize model complexes $[Ni^{II}(L)(P\text{-}(o\text{-}C_6H_4S)_2(o\text{-}C_6H_4\text{-}SH))]^{0/1-}$ (L = PPh_3 (**1**), SePh (**4**), Se-*p*-C_6H_4-Cl (**5**), and Cl (**6**)) and $[Ni^{II}(L')(P(o\text{-}C_6H_4S)_2(o\text{-}C_6H_4\text{-}SCH_3))]^{0/1-}$ (L′ = PPh_3 (**8**), SPh (**9**), SePh (**10**)) with various electron-donating ligands, L/L′, coordinated to the nickel center. This study further provides evidence that the pendant thiol proton of the Ni(II) complexes, $[Ni^{II}(L)(P\text{-}(o\text{-}C_6H_4S)_2(o\text{-}C_6H_4SH))]^{0/1-}$, were "arrested" by both the sulfur of thiolate and nickel resulting in combinations of intramolecular [Ni−S···H−S] and [Ni···H−S] interactions, and the extent of the interactions was modulated by the monodentate ligand.

Results and Discussion

Synthesis of Ni(II)−Thiol Complex $[Ni^{II}(PPh_3)(P\text{-}(o\text{-}C_6H_4S)_2(o\text{-}C_6H_4SH))]$ (1). Reaction of $NiCl_2(PPh_3)_2$ and tris-(2-phenylthiol)phosphine ($P(o\text{-}C_6H_4SH)_3$) in THF at ambient temperature led to the isolation of the red-brown four-

(5) (a) Higuchi, Y.; Yagi, T.; Yasuoka, N. *Structure* **1997**, *5*, 1671−1680. (b) Higuchi, Y.; Ogata, H.; Miki, K.; Yasuoka, N.; Yagi, T. *Structure* **1999**, *7*, 549−556. (c) Ogata, H.; Mizoguchi, Y.; Mizuno, N.; Miki, K.; Adachi, S.-I.; Yasuoka, N.; Yagi, T.; Yamauchi, O.; Hirota, S.; Higuchi, Y. *J. Am. Chem. Soc.* **2002**, *124*, 11628−11635. (d) Foerster, S.; Stein, M.; Brecht, M.; Ogata, H.; Higuchi, Y.; Lubitz, W. *J. Am. Chem. Soc.* **2003**, *125*, 83−93.

(6) Rousset, M.; Montet, Y.; Guigliarelli, B.; Forget, A.; Asso, M.; Bertrand, P.; Fontecilla-Camps, J. C.; Hatchikian, E. C. *Proc. Natl. Acad. Sci. U.S.A.* **1998**, *95*, 11625−11630.

(7) Matias, P. M.; Soares, C. M.; Saraiva, L. M.; Coelho, R.; Morais, J.; Le Gall, J.; Carrondo, M. A. *J. Biol. Inorg. Chem.* **2001**, *6*, 63−81.

(8) (a) De Lacey, A. L.; Hatchikian, E. C.; Volbeda, A.; Frey, M.; Fontecilla-Camps, J. C.; Fernandez, V. M. *J. Am. Chem. Soc.* **1997**, *119*, 7181−7189. (b) Maroney, M. J.; Davidson, G.; Allan, C. B.; Figlar, J. S*truct. Bonding* **1998**, *92*, 1−65. (c) Bagley, K. A.; Duin, E. C.; Roseboom, W.; Albracht S. P. J.; Woodruff, W. H. *Biochemistry* **1995**, *34*, 5527. (d) Coremans, J. M. C. C.; van der Zwaan, G. W.; Albracht, S. P. J. *Biochim. Biophys. Acta* **1992**, *1119*, 157−168. (e) Stein, M.; Lubitz, W. *Curr. Opin. Chem. Biol.* **2002**, *6*, 243−249.

(9) Niu, S.; Thomson, L. M.; Hall, M. B. *J. Am. Chem. Soc.* **1999**, *121*, 4000−4007.

(10) De Gioia, L.; Fantucci, P.; Guigliarelli, B.; Bertrand, P. *Inorg. Chem.* **1999**, *38*, 2658−2662.

(11) (a) Fan, C.; Teixeira, M.; Moura, J.; Moura, I.; Huynh, B. H.; Le Gall, J.; Peck, H. D., Jr.; Hoffman, B. M. *J. Am. Chem. Soc.* **1991**, *113*, 20−24. (b) Whitehead, J. P.; Gurbiel, R. J.; Bagyinka, C.; Hoffman, B. M.; Maroney, M. J. *J. Am. Chem. Soc.* **1993**, *115*, 5629−5635.

(12) Foerster, S.; van Gastel, M.; Brecht, M.; Lubitz, W. *J. Biol. Inorg. Chem.* **2005**, *10*, 51−62.

(13) (a) Darensbourg, M. Y.; Lyon, E. J.; Smee, J. *Coord. Chem. Rev.* **2000**, *206*, 533−561. (b) Allan, C. B.; Davidson, G.; Choudhury, S. B.; Gu, Z.; Bose, K.; Day, R. O.; Maroney, M. J. *Inorg. Chem.* **1998**, *37*, 4166−4167. (c) James, T. L.; Cai, L.; Mutterties, M. C.; Holm, R. H. *Inorg. Chem.* **1996**, *35*, 4148−4161. (d) Cha, M.; Shoner, S. C.; Kovacs, J. A. *Inorg. Chem.* **1993**, *32*, 1860−1863. (e) Nguyen, D. H.; Hsu, H.-F.; Millar, M.; Koch, S. A.; Achim, C.; Bominaar, E. L.; Munck, E. *J. Am. Chem. Soc.* **1996**, *118*, 8963−8964. (f) Bouwman, E.; Reedijk, J. *Coord. Chem. Rev.* **2005**, *249*, 1555−1581.

(14) Alvarez, H. M.; Krawiec, M.; Donovan-Merkert, B. T.; Fouzi, M.; Rabinovich, D. *Inorg. Chem.* **2001**, *40*, 5736−5737.

(15) Zimmer, M.; Schulte, G.; Luo, X.-L.; Crabtree, R. H. *Angew. Chem., Int. Ed. Engl.* **1991**, *30*, 193−194.

(16) Clegg, W.; Henderson, R. A. *Inorg. Chem.* **2002**, *41*, 1128−1135.

(17) Li, Z.; Ohki, Y.; Tatsumi, K. *J. Am. Chem. Soc.* **2005,** *127*, 8950−8951.

Scheme 1

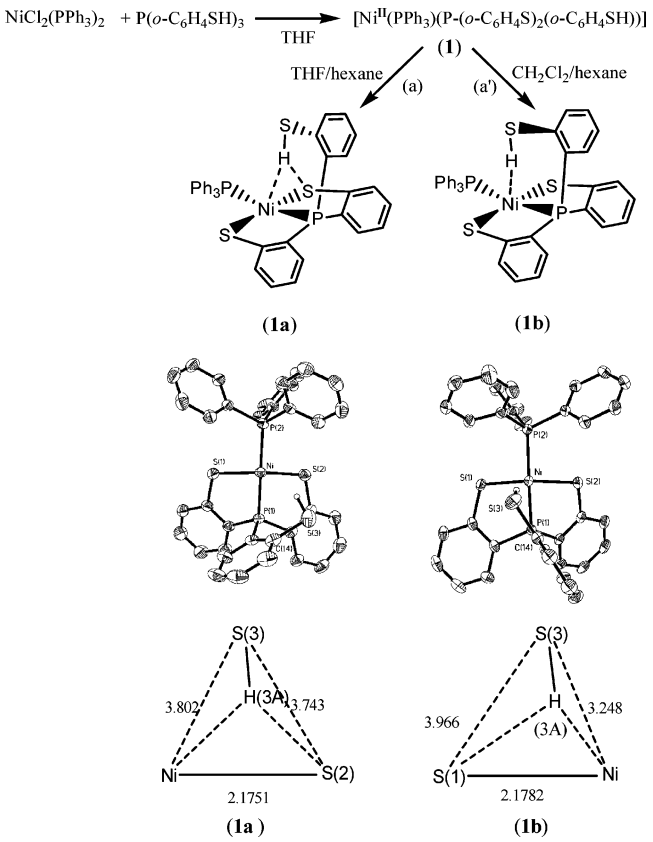

coordinated Ni(II) complex, **1**, in a high yield (79%) (Scheme 1).[18,19] Complex **1** is soluble in CH_2Cl_2/THF and displays air sensitivity in organic solvents. However, in the solid state, complex **1** is air-stable for minutes. The ^{1}H NMR spectrum of complex **1** displays the benzene proton resonances at 6.993 (t), 7.181 (t), 7.293−7.424 (m), 7.708 (t) ppm, and the ^{31}P NMR spectrum shows two nonequivalent phosphorus atoms at 76.57 (d) ($J_{^{31}P-^{31}P}$ = 695 Hz, (P-(*o*-C$_6$H$_4$S)$_2$(*o*-C$_6$H$_4$SH)) and 24.65 (d) ($J_{^{31}P-^{31}P}$ = 695 Hz, PPh_3) ppm (vs H_3PO_4) ($CDCl_3$). Both the ^{1}H and ^{31}P NMR spectra are consistent with a low-spin d^8 Ni(II) electronic configuration in a square-planar ligand field. The chemical shift (5.91 ppm (S−H) ($CDCl_3$)) of the pendant thiol of complex **1** is shifted ca. 1.84 ppm downfield from that of the free thiol P(*o*-C$_6$H$_4$-SH)$_3$ (δ 4.07 (d)).[19] Treatment of complex **1** with D_2O in a THF solution at 5 °C led to the H/D exchange product [Ni^{II}(PPh$_3$)(P(*o*-C$_6$H$_4$S)$_2$(*o*-C$_6$H$_4$SD))] (**1-D**), identified by IR and ^{2}H NMR. The IR ν_{S-D} stretching frequency of 1752 (br) cm^{-1} ($\nu_{S-D,}$ KBr) for complex **1-D** is consistent with the calculated position, based only on the difference in masses between S−H and S−D. The ^{2}H NMR spectrum of complex **1-D** (using the natural abundance of D in C_4H_8O solvent, two singlet peaks at 1.73 and 3.57 ppm, as internal standard) displaying the signal at 6.175 (br) ppm (C_4H_8O) was assigned to the S−D resonance. When a THF solution of complex **1** was recrystallized with THF−hexane, complex **1a**, displaying a broad ν_{S-H} stretching band at 2393 cm^{-1} (KBr), was isolated and characterized by X-ray crystallography (Scheme 1). In contrast, the diffusion of hexane into a CH_2Cl_2 solution of complex **1** yielded complex **1b** with a broad ν_{S-H} stretching band at 2240 cm^{-1} (KBr), characterized by single-crystal diffraction (Scheme 1). The IR spectra of complexes **1a** and **1b** display broad ν_{S-H} stretching bands at 2393 and 2240 cm^{-1} (KBr), which are ∼90 and ∼250 cm^{-1}, respectively, lower than the free ligand, 2488 cm^{-1} (KBr). This lower ν_{S-H} stretching frequency may imply the existence of intramolecular [Ni−S···H−S]/[Ni···H−S] interactions.[18]

The ORTEP diagrams of complexes **1a** and **1b** are shown in Figure 1. The selected bond distances and angles are given in the figure caption. Complexes **1a** and **1b** consist of a four-coordinate nickel(II) center in a distorted square planar geometry with two thiolate sulfur atoms and two phosphorus atoms, respectively, in the trans positions. In complex **1a**, the acute (C(14)−S(3)−H(3A)) bond angle of 95.04° and the similar distances of Ni···S(3) (3.802 Å) and S(2)···S(3) (3.743 Å) suggested that the proton of S(3)−H(3A) points toward the middle, between the Ni and S(2) atoms, and interacts with both the sulfur (S(2)) and nickel atoms (i.e., a combination of the intramolecular [Ni−S···H−S] and

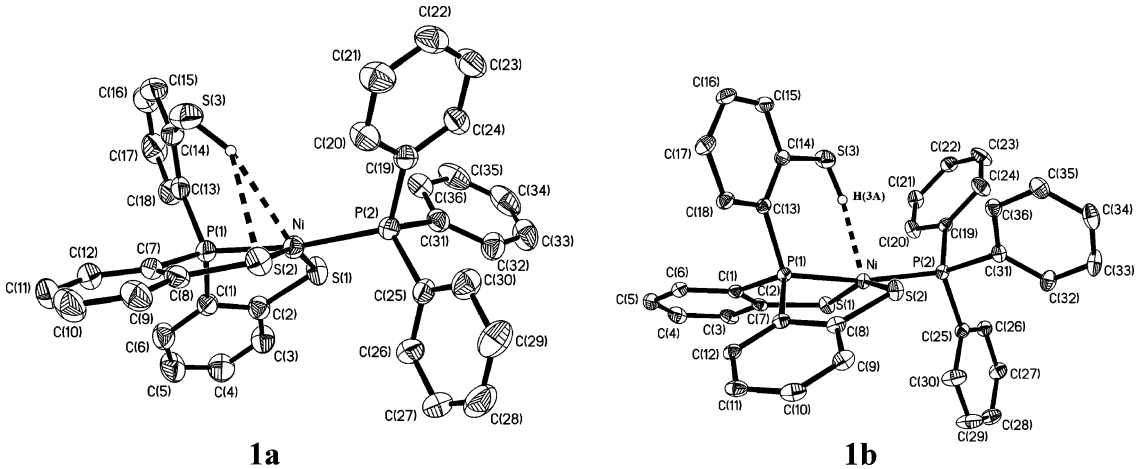

Figure 1. ORTEP drawing and labeling scheme of [Ni^{II}(PPh$_3$)(P(*o*-C$_6$H$_4$S)$_2$(*o*-C$_6$H$_4$SH))] (**1a** and **1b**). Selected bond distances (Å) and angles (deg): complex **1a** Ni−S(1) = 2.1892(9), Ni−S(2) = 2.1751(9), Ni−P(1) = 2.1318(8), Ni−P(2) = 2.2452(8), S(1)−Ni−S(2) = 156.68(4), P(1)−Ni−P(2) = 171.64, S(1)−Ni−P(2) = 94.66(3), S(2)−Ni−P(2) = 93.85(3), C(1)−P(1)−Ni = 106.37(10), C(7)−P(1)−Ni = 110.05(11), C(13)−P(1)−Ni = 117.02(9); complex **1b** Ni−S(1) = 2.1782(5), Ni−S(2) = 2.1916(5), Ni−P(1) = 2.1224(5), Ni−P(2) = 2.2340(5), S(1)−Ni−S(2) = 156.01(2), P(1)−Ni−P(2) = 169.75(2), S(1)−Ni−P(2) = 94.88(2), S(2)−Ni−P(2) = 94.82(2), C(1)−P(1)−Ni = 110.33(7), C(7)−P(1)−Ni = 106.60(6), C(13)−P(1)−Ni = 116.50(6).

Scheme 2

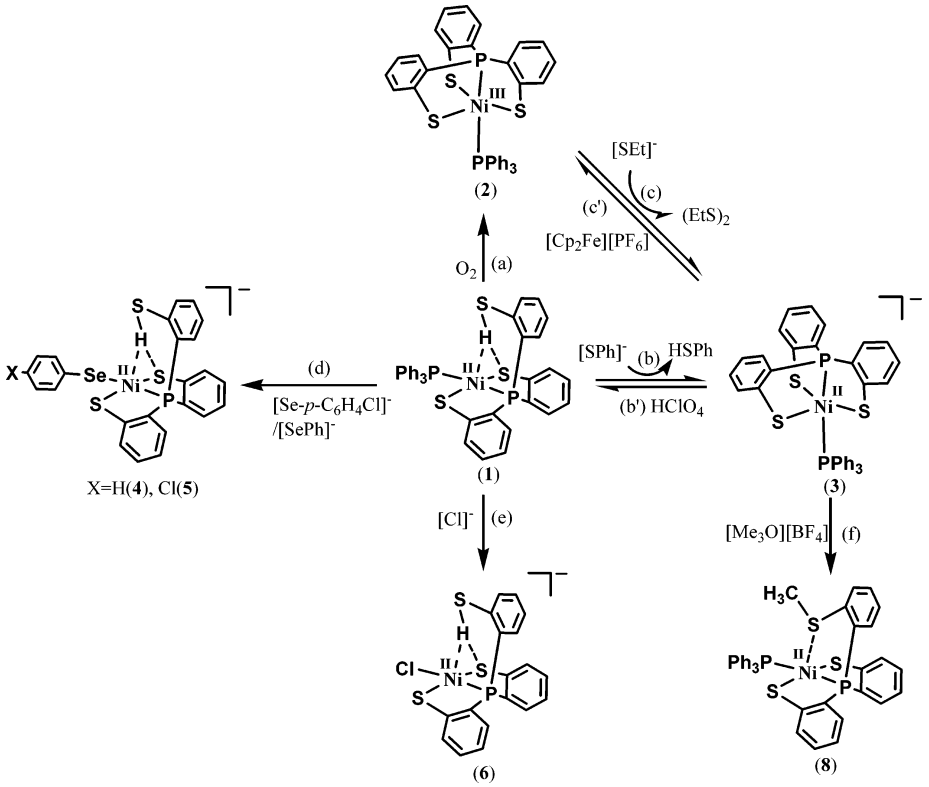

[Ni···H−S] interactions, Scheme 1). In contrast, the Ni···S(3) distance of 3.248 Å is significantly shorter than the S(1)···S(3) distance of 3.966 Å in complex **1b**. Also, the Ni−P(1)−C(13)−C(14) torsion angle of 35.2° observed in complex **1b** is significantly smaller than the Ni−P(1)−C(13)−C(14) torsion angle of 62.6° observed in complex **1a** (Scheme 1). Compared to complex **1a**, the acute C(14)−S(3)−H(3A) bond angle of 99.64°, the smaller Ni−P(1)−C(13)−C(14) torsion angle of 35.2°, and a lower ν_{S-H} stretching band (2240 cm^{-1} (KBr)) may indicate that the thiol proton tends to interact directly with the nickel atom in complex **1b** (i.e., a [Ni···H−S] interaction). We noticed that the most probable Ni···H(3A)−S distance of 2.182 Å in complex **1b** is roughly consistent with the Ni···H−B distance of 1.863 Å in complex $Ni^{II}(Bm^{Me})_2$.[14] The pendant thiol interaction modes in the solid state (complexes **1a** and **1b**, Scheme 1) may be controlled by the solvent of crystallization.

Syntheses of Complexes $[Ni^{III}(PPh_3)(P(o\text{-}C_6H_4S)_3)]$ (2) and $[PPN][Ni^{II}(PPh_3)(P(o\text{-}C_6H_4S)_3)]$ (3). When dry O_2 was added to the THF solution of complex **1** at 0 °C, a color change from red-brown to dark green was observed (Scheme 2a). As observed in the previous study,[18] the reaction led to the formation of complex **2** accompanied by the byproduct H_2O, characterized by UV−vis, ^{1}H NMR, SQUID, and single-crystal X-ray diffraction. The formation of the byproduct, H_2O, was confirmed again by treating a dry THF solution of complex **1-D** with dry O_2 at ambient temperature. The ^{2}H NMR spectrum shows the expected signal at 2.783 ppm (br) for the byproduct D_2O, and the UV−vis spectra display the characteristic absorption bands (610, 672, and 1152 nm (CH_2Cl_2)) of complex **2**. Complex **2** is soluble in CH_2Cl_2/THF and displays air and thermal sensitivity. The ^{1}H NMR spectrum of complex **2** displays the paramagnetic chemical shifts at −3.99 (br), 5.48 (br), 8.42 (br), 9.70 (br), 11.82 (br), 12.62 (br), and 13.67 (br) ppm ($CDCl_3$) at 298 K, and the effective magnetic moment in the solid state, found using the the SQUID magnetometer, is 1.71 μ_B. These results support the idea that complex **2** adopts a low-spin d^7 Ni(III) electronic configuration in a distorted trigonal bipyramidal ligand field. The cyclic voltammogram of complex **2** (measured in a 2 mM CH_2Cl_2 solution of complex **2**, with 0.1 M [*n*-Bu_4N][PF_6] as the supporting electrolyte at room temperature, scan rate 100 mV/s) reveals one reversible reduction−oxidation process (i.e., reversible Ni(III)−Ni(II) redox process) at $E_{1/2}$ = −0.865 V (vs Cp_2Fe/Cp_2Fe^+) (Figure 2).

When a CH_3CN−THF (1:3 volume ratio) solution of complex **1** and $[SPh]^-$ (or $[SEt]^-$) was stirred at ambient temperature for 3 h (Scheme 2b), a deprotonation reaction occurred yielding mononuclear complex **3** accompanied by the liberation of thiophenol (or ethanethiol), identified by ^{1}H NMR spectra; protonation of complex **3** in THF at 0 °C by $HClO_4$ produced complex **1** (Scheme 2b′), characterized by IR and ^{1}H NMR spectra. Instead of ligand displacement, treatment of complex **2** with 1 equiv of $[SEt]^-$ in CH_3CN−THF solutions (1:3 volume ratio) for 1.5 h at ambient temperature led to the reduction of complex **2** to produce complex **3** and diethyl disulfide, identified by ^{1}H NMR (Scheme 2c). Complex **3** is soluble in CH_2Cl_2 or CH_3CN−THF (1:3 volume ratio), but it is significantly less soluble

(18) Lee, C.-M.; Chen, C.-H.; Ke, S.-C.; Lee, G.-H.; Liaw, W.-F. *J. Am. Chem. Soc.* **2004**, *126*, 8406−8412.
(19) Block, E.; Ofori-Okai, G.; Zubieta, J. *J. Am. Chem. Soc.* **1989**, *111*, 2327−2329.

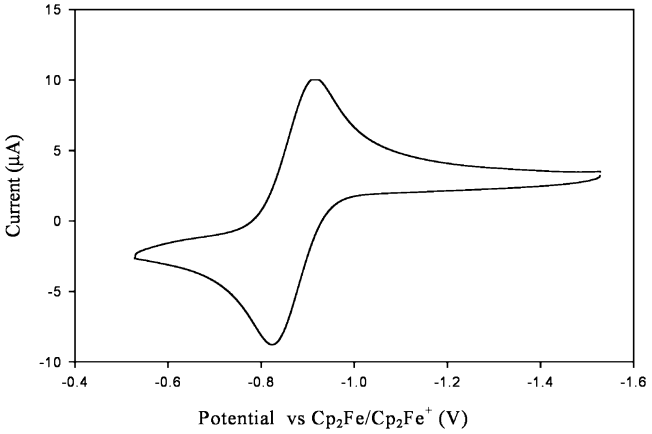

Figure 2. Cyclic voltammogram of [Ni^{III}(PPh$_3$)(P(*o*-C$_6$H$_4$S)$_3$)] (**2**) (measured in a 2 mM CH_2Cl_2 solution with 0.1 M [*n*-Bu$_4$N][PF$_6$] as the supporting electrolyte at room temperature, scan rate 100 mV/s) vs Cp$_2$Fe/Cp$_2$Fe$^+$ (ΔE_p = 0.087 V).

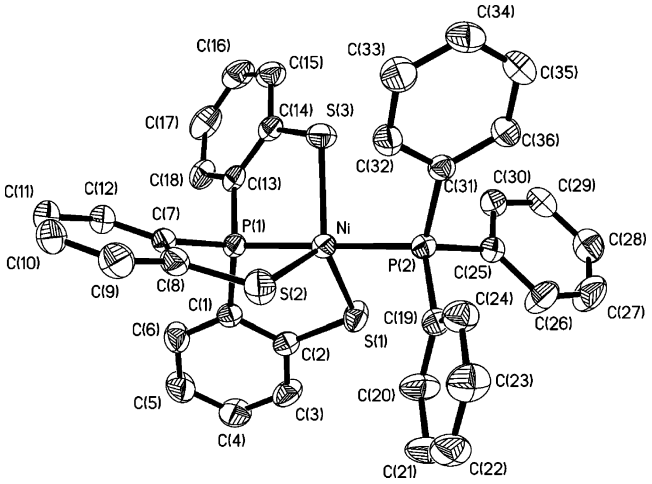

Figure 3. ORTEP drawing and labeling scheme of [Ni^{III}(PPh$_3$)(P(*o*-C$_6$H$_4$S)$_3$)] (**2**). Selected bond distances (Å) and angles (deg): Ni−P(1) = 2.1270(10), Ni−P(2) = 2.2519(10), Ni−S(1) = 2.2392(11), Ni−S(2) = 2.3010(12), Ni−S(3) = 2.2564(11), P(1)−Ni−P(2) = 178.73(4), P(1)−Ni−S(1) = 86.36(4), P(2)−Ni−S(1) = 94.64(4), S(1)−Ni−S(2) = 117.66(5), S(1)−Ni−S(3) = 126.01(5), S(2)−Ni−S(3) = 114.57(5).

in pure THF or pure CH_3CN. The CH_2Cl_2 solution of complex **3** is air sensitive. The ^{1}H NMR spectrum of complex **3** is consistent with low-spin d^8 Ni(II). Complex **2** was regenerated upon addition of [Cp$_2$Fe][PF$_6$] to complex **3** in CH_3CN at 0 °C, based on the disappearance of the 801 nm absorption band (CH_2Cl_2) and the concomitant formation of 611 and 671 nm absorption bands of complex **2** (Scheme 2c′). Apparently, complexes **2** and **3** are chemically interconvertible without decomposition. During the reversible reduction/oxidation of complexes **2**/**3**, the retention of the coordination number and geometry of the nickel ion and the prevention of a potential dimerization from removing the triphenylphosphine ligand suggest that the one phosphine and three thiolate ligands coordinated to Ni(III)/Ni(II) may optimize the electronic structure of the nickel ion to stabilize complexes **2** and **3**.

X-ray crystal structures of complexes **2** and **3** are depicted in Figures 3 and 4, respectively, and selected bond coordinates for complexes **2** and **3** are presented in the figure captions. Complex **2** is essentially isostructural with complex **3**. The geometry of the Ni center is a trigonal bipyramidal

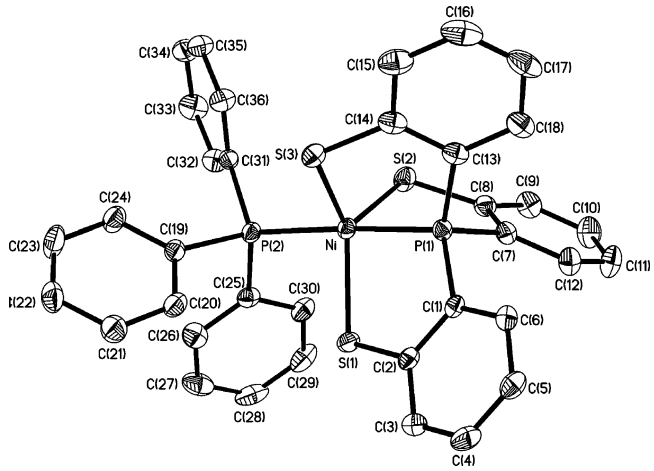

Figure 4. ORTEP drawing and labeling scheme of [Ni^{II}(PPh$_3$)(P(*o*-C$_6$H$_4$S)$_3$)]$^-$ anion (**3**). Selected bond distances (Å) and angles (deg): Ni−P(1) = 2.0995(7), Ni−P(2) = 2.1978(7), Ni−S(1) = 2.2801(7), Ni−S(2) = 2.3729(8), Ni−S(3) = 2.3056(8), P(1)−Ni−P(2) = 177.00(3), P(1)−Ni−S(1) = 85.12(3), P(2)−Ni−S(1) = 92.19(3), S(1)−Ni−S(2) = 121.17(3), S(1)−Ni−S(3) = 120.77(3), S(2)−Ni−S(3) = 115.62(3).

with three thiolate sulfurs in the equatorial positions and two phosphorus atoms in the axial positions for both complexes **2** and **3**. The strained effect of the chelating ligand from the tridentate mode in complex **1** to the tetradentate mode in complex **3** results in an increase of mean Ni−S bond distances of 0.137 Å. Compared to Ni(II) complex **1**, the mean Ni−S distance in Ni(III) complex **2** increased by 0.082 Å. Obviously, the longer Ni−S bond distances in complex **2** indicate that the influence of the strained effect of the chelating ligand overwhelms the contraction effect resulting from the oxidation of Ni(II) (complexes **1**/**3**) to Ni(III) (complex **2**). Reduction of complex **2** to **3** (Ni(III) to Ni(II)) was believed to cause the elongation of the mean Ni−S bond distances (mean Ni−S bond distances: 2.266 Å for **2**, 2.320 Å for **3**). In complex **2**, the nickel atom lies 0.174 Å under the mean plane defined by three sulfur atoms toward the axial triphenyl phosphine. The displaced distance (0.2102 Å) of the nickel atom from the mean three sulfur atom plane toward the axial triphenyl phosphine was observed in complex **3**.

Preparation of Ni(II)−Thiol Derivatives by Ligand Displacement. In contrast to the deprotonation of complex **1** by addition of the anionic thiolates [PhS]$^-$/[SEt]$^-$, the addition of [SePh]$^-$ (or [Cl]$^-$/[Se-*p*-C$_6$H$_4$−Cl]$^-$) to the CH_3CN−THF solution (1:3 volume ratio) of complex **1** at 0 °C for 4 h yielded ligand-displacement complexes, [Ni^{II}(L)(P-(*o*-C$_6$H$_4$S)$_2$(*o*-C$_6$H$_4$SH))]$^-$ (L = SePh (**4**), Se-*p*-C$_6$H$_4$−Cl (**5**), Cl (**6**)), isolated as red-brown solids and identified by IR, NMR, UV−vis, and single-crystal X-ray diffraction (Scheme 2d and 2e).[18] Reaction of complex **1** and stronger (hard) Lewis base ligands ([PhS]$^-$ and [SEt]$^-$) triggers deprotonation of complex **1** to yield complex **3**. However, the reaction of complex **1** and weaker (soft) Lewis base ligands ([SePh]$^-$, [Se-*p*-C$_6$H$_4$−Cl]$^-$, [Cl]$^-$) preferred the ligand-displacement reaction to produce complexes **4**−**6**. Complex **6** is soluble in CH_2Cl_2 and CH_3CN−THF (1:3 volume ratio) and is air sensitive. The IR spectrum of complex **6** displays the ν_{S-H} stretching band at 2300 cm^{-1}(KBr) which is ∼150 cm^{-1} lower than that of the free

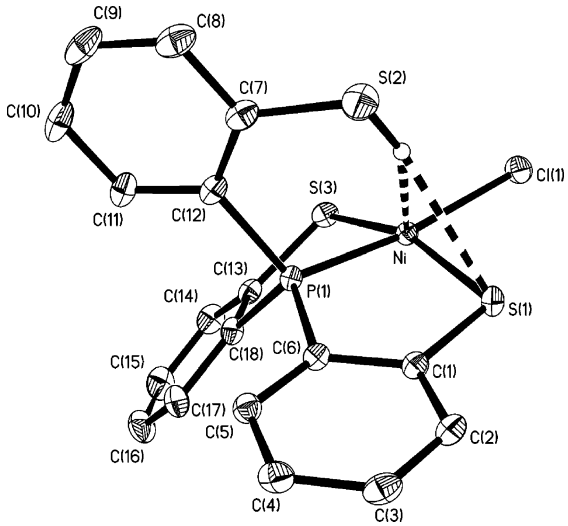

Figure 5. ORTEP drawing and labeling scheme of the $[Ni^{II}Cl(P(o\text{-}C_6H_4S)_2(o\text{-}C_6H_4SH))]^-$ anion (**6**). Selected bond distances (Å) and angles (deg): Ni−S(1) = 2.1783(7), Ni−S(3) = 2.2111(8), Ni−P(1) = 2.0891(7), Ni−Cl(1) = 2.2243(7), S(1)−Ni−S(3) = 161.36(3), P(1)−Ni−Cl(1) = 170.89(3), S(1)−Ni−Cl(1) = 91.93(3), S(3)−Ni−Cl(1) = 95.74(3), C(18)−P(1)−Ni = 106.63(9), C(6)−P(1)−Ni = 110.44(9), C(12)−P(1)−Ni = 116.20(10).

Table 1. IR ν_{S-H} Stretching Frequencies for Complexes **1a**, **1b**, **4**, **5**, **6**, and **7**

complex	ν(S−H), cm^{-1} (KBr)
L = PPh_3 (**1a**)	2393
L = Cl (**6**)	2300
L = Se-*p*-C_6H_4−Cl (**5**)	2288
L = S−C_4H_3S (**7**)	2283
L = SePh (**4**)	2273
L = PPh_3 (**1b**)	2240

ligand $P(o\text{-}C_6H_4SH)_3$, and the ^{1}H NMR spectrum of complex **6** shows the downfield chemical shift of the SH group at 5.808 (s) ppm ($CDCl_3$), suggesting the existence of an intramolecular [Ni−S···H−S] interaction (or presumably, a combination of [NiS···H−S] and [Ni···H−S] interactions).

Figure 5 displays an ORTEP plot of the anionic mononuclear complex **6**, and the selected bond distances and angles are presented in figure caption. The single-crystal X-ray structural analysis of complex **6**, isostructural with complex **5**, reveals that the geometry of Ni(II) in complex **6** is a distorted square planar with a phosphorus, a chloride and two trans thiolate ligands. The large C(12)−P(1)−Ni angle of 116.20(10)° differs from the C(6)−P(1)−Ni and C(18)−P(1)−Ni angles of 110.44(9)° and 106.63(9)° in complex **6**. The acute (C(12)−S(2)−H(2S)) bond angle of 99.89° and the similar distances of Ni···S(2) (3.642 Å) and S(1)···S(2) (3.698 Å) also suggested that the specific intramolecular [Ni−S···H−S] interaction exists in complex **6**.

As shown in Table 1, the IR ν_{S-H} stretching frequencies for complexes **1a**, **4**, **5**, **6**, and $[Ni^{II}(S\text{-}C_4H_3S)(P\text{-}(o\text{-}C_6H_4S)_2(o\text{-}C_6H_4SH))]^-$ (**7**) reflect the expected changes as the electron-donating abilities of the monodentate ligands $[SePh]^-$, $[S-C_4H_3S]^-$, $[Se\text{-}p\text{-}C_6H_4-Cl]^-$, $[Cl]^-$, and PPh_3 are varied.[18] The IR ν_{S-H} stretching frequencies of complexes **1a**, **4**, **5**, **6**, and **7** clearly revealed that the stronger electron-donating monodentate ligands enriched the electronic density of the Ni(II) and sulfur centers triggering the stronger pendant thiol proton interacting with both Ni(II) and thiolate sulfur to result in the weaker S−H bond strength. The above results unambiguously illustrate one aspect of how a coordinated ligand functions to promote [Ni−S···H−S] interactions (or a combination of [Ni−S···H−S] and [Ni···H−S] interactions).

Syntheses of Ni(II)−Thioether Complexes. To further corroborate the pendant thiol proton interacting with the sulfur atom (or presumably, both the sulfur and nickel atoms) in **1a**, **1b**, and **4**−**7**, where the proton is bound to sulfur and "attracted" by the second sulfur atom to yield an intramolecular [Ni−S···H−S] interaction, the neutral $[Ni^{II}(PPh_3)(P(o\text{-}C_6H_4S)_2(o\text{-}C_6H_4\text{-}SCH_3))]$ (**8**) complex was synthesized. As shown in Scheme 2f, treatment of $[Me_3O][BF_4]$ and complex **3** in a CH_3CN−THF solution (1:3 volume ratio) at 0 °C for 4 h yielded the green solid, $[Ni^{II}(PPh_3)(P(o\text{-}C_6H_4S)_2(o\text{-}C_6H_4\text{-}SCH_3))]$ (**8**), identified by NMR, UV−vis, and single-crystal X-ray diffraction. Complex **8** is soluble in THF and CH_2Cl_2, but it is insoluble in hexane, CH_3CN, and MeOH. The ^{1}H NMR spectrum of complex **8** exhibits the methyl (CH_3) proton resonance at 2.021 ppm, and the ^{31}P NMR spectrum shows two nonequivalent phosphorus atoms at 84.423 (d) ($J_{^{31}P-^{31}P}$ = 649 Hz) and 26.639 ppm (d) ($J_{^{31}P-^{31}P}$ = 649 Hz, PPh_3) (vs H_3PO_4) ($CDCl_3$) at room temperature. Both the ^{1}H NMR and ^{31}P NMR spectra are consistent with a low-spin d^8 Ni(II) complex in a square planar ligand field. However, the temperature dependence of the ^{1}H NMR spectrum of complex **8** revealed that the chemical shifts of the methyl group change from 1.820 ppm at −60 °C to 2.109 ppm at 60 °C (C_4D_8O) (Supporting Information). On the basis of the single-crystal X-ray diffraction, two different conformational isomers were isolated. The green crystals of complex **8a** were obtained by diffusion of hexane into the THF solution of complex **8** at 0 °C. Interestingly, the diffusion of hexane into the THF solution of complex **8** at 30 °C produced green crystals (complex **8a**) and red crystals which were identified by single-crystal X-ray diffraction as complex **8b**. Each crystal form shows identical ^{1}H NMR spectroscopic properties (methyl (CH_3) proton resonance at 2.021 ppm) ($CDCl_3$)) when complexes **8a** and **8b** were redissolved in $CDCl_3$ at room temperature. Obviously, these two conformational isomers (**8a** and **8b**) are in equilibrium with one another via intramolecular rearrangement controlled by the temperature in solution.

Figure 6 displays ORTEP plots of complexes **8a** and **8b**, respectively. The nickel center is best described as existing in a distorted square planar coordination environment surrounded by two trans thiolate sulfur atoms and two phosphorus atoms. The selected bond distances and angles are given in the caption of Figure 6. The increase in the Ni···S(3) distance of ca. 0.37 Å from complex **8a** to **8b** has several consequences. The torsion angles of Ni−P(1)−C(13)−C(18) are 6.5 and 24.9° in complexes **8a** and **8b**, respectively. The C(13)−P(1)−Ni angle of 115.76(11)° differs from the C(1)−P(1)−Ni and C(7)−P(1)−Ni angles of 110.65(11)° and 107.38(10)° in complex **8b**. In contrast, complex **8a** shows similar bond angles, ∠C(7)−P(1)−Ni = 110.82(11), ∠C(1)−P(1)−Ni = 111.19(12), and ∠C(13)−P(1)−Ni = 111.09(12)°. The Ni−S(3)−C(19) bond angles of 109° in complex **8a**

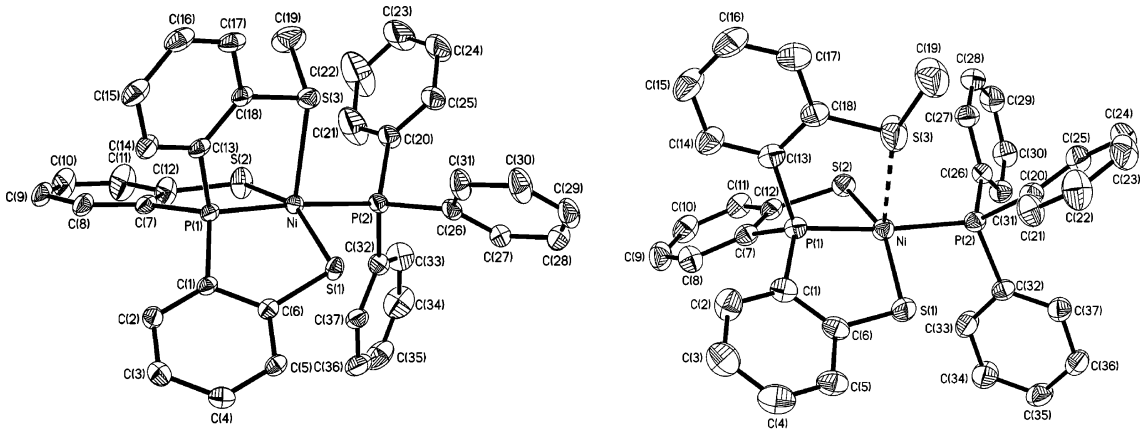

Figure 6. ORTEP drawing and labeling scheme of [Ni^{II}(PPh$_3$)(P(*o*-C$_6$H$_4$S)$_2$(*o*-C$_6$H$_4$-SCH$_3$))] (**8a**) and [Ni^{II}(PPh$_3$)(P(*o*-C$_6$H$_4$S)$_2$(*o*-C$_6$H$_4$-SCH$_3$))] (**8b**). Selected bond distances (Å) and angles (deg): complex **8a** Ni−S(1) = 2.2150(11), Ni−S(2) = 2.2281(10), Ni−P(1) = 2.1209(10), Ni−P(2) = 2.2323(10), Ni···S(3) = 2.5397(10), S(1)−Ni−S(2) = 147.99(4), P(1)−Ni−P(2) = 177.31(4), S(1)−Ni−P(2) = 90.01(4), S(2)−Ni−P(2) = 94.39(4), C(7)−P(1)−Ni = 110.82(12), C(1)−P(1)−Ni = 111.19(12), C(13)−P(1)−Ni = 111.09(12), C(18)−S(3)−C(19) = 99.30(19), Ni−S(3)−C(19) = 109.00(17); complex **8b** Ni−S(1) = 2.1828(9), Ni−S(2) = 2.2044(8), Ni−P(1) = 2.1160(8), Ni−P(2) = 2.2343(8), Ni···S(3) = 2.9135(11), S(1)−Ni−S(2) = 153.42(4), P(1)−Ni−P(2) = 173.33, S(1)−Ni−P(2) = 93.22(3), S(2)−Ni−P(2) = 95.55(3), C(1)−P(1)−Ni = 110.65(11), C(7)−P(1)−Ni = 107.38(10), C(13)−P(1)−Ni = 115.76(11), Ni−S(3)−C(19) = 158.18(19), C(18)−S(3)−C(19) = 103.7(2).

Scheme 3

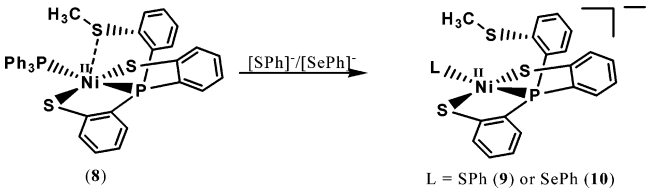

and 158.18° in complex **8b** demonstrate that the methyl groups of these Ni(II) complexes, **8a**/**8b**, do not point directly to the Ni or S atoms. These results further support that the pendant thiol proton of the Ni(II)−thiol complexes, **1a**/**4**−**7**, locates in the position attracted by both nickel and the sulfur of thiolate to stabilize the thiol proton. Compared to the Ni···S(3) distances of 3.802 and 3.248 Å observed in complexes **1a** and **1b** (Scheme 1), the single-crystal X-ray structure revealed that a thioether sulfur semibonding to Ni(II) (Ni···S(3) distances of 2.5397 Å) may exist in complex **8a**, and there is no interaction between Ni and S(3) (Ni···S(3) distances of 2.9135 Å) in complex **8b**. The electron back-donation of Ni(II) to the π-accepting thioether sulfur may be adopted to rationalize the upfield chemical shift of the methyl group in complex **8a** (green crystals obtained at 0 °C or lower),[20] as compared to complex **8b** (red crystals obtained at 30 °C).

In contrast to the temperature-dependent interconversion of the conformational isomers **8a** and **8b**, the temperature-independent four-coordinated Ni(II)−thioether complexes [Ni^{II}(L)(P(*o*-C$_6$H$_4$S)$_2$(*o*-C$_6$H$_4$-SCH$_3$))]$^-$ (L = SPh (**9**), SePh (**10**)) were isolated when complex **8** was reacted with [SPh]$^-$/[SePh]$^-$ in THF at room temperature overnight, respectively (Scheme 3). The red brown complexes **9** and **10** are soluble in THF, CH_2Cl_2, and CH_3CN. The ^{1}H NMR spectra of

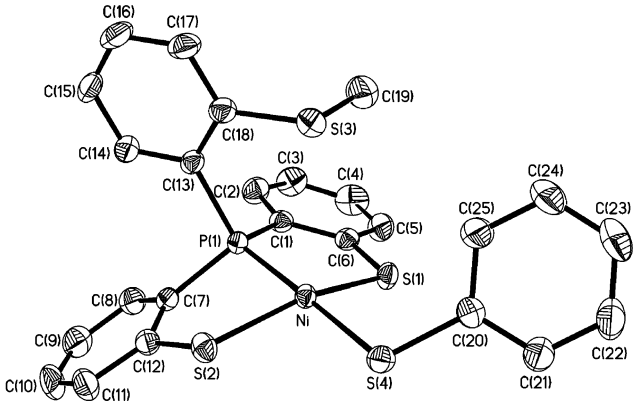

Figure 7. ORTEP drawing and labeling scheme of the [Ni^{II}(SPh)(P(*o*-C$_6$H$_4$S)$_2$(*o*-C$_6$H$_4$−SCH$_3$))]$^-$ anion (**9**). Selected bond distances (Å) and angles (deg): Ni−S(1) = 2.1664(7), Ni−S(2) = 2.2187(7), Ni−P(1) = 2.0998(7), Ni−S(4) = 2.2322(7), Ni···S(3) = 3.258(7), S(1)−Ni−S(2) = 159.61(3), P(1)−Ni−S(4) = 176.97(3), S(1)−Ni−S(4) = 93.79(3), S(2)−Ni−S(4) = 91.82(3), C(7)−P(1)−Ni = 106.73(9), C(1)−P(1)−Ni = 110.53(9), C(13)−P(1)−Ni = 119.48(9), C(18)−S(3)−C(19) = 100.66(15), Ni−S(3)−C(19) = 102.47(15).

complexes **9** and **10** are consistent with the diamagnetic d^8 square planar Ni(II) complexes, and the chemical shifts at 2.528 (s) and 2.553 (s) ppm ($CDCl_3$) were assigned to the methyl groups of complexes **9** and **10**, respectively. Presumably, there is no interaction between Ni(II) and the thioether sulfur atom (Ni···S(3) distance of 3.258(7) and 3.229 (5) Å in complexes **9** and **10**, respectively); therefore, the absence of electron back-donation of Ni(II) to the π-accepting thioether sulfur may explain the downfield chemical shift of the methyl groups in complexes **9** and **10**, as compared to complexes **8a** and **8b**.

Figures 7 shows the thermal ellipsoid plot of the anionic complex **9**, and the selected bond distances and angles of complex **9** are given in the figures caption, respectively. Complexes **9** and **10** are isostructural Ni(II) complexes with the monodentate thiolate/selenolate ligands. The Ni···S$_{(thioether)}$ distances of 3.258(7) and 3.229 (5) Å found in complexes **9**

(20) (a) Ashby, M. T.; Enemark, J. H.; Lichtenberger, D. L. *Inorg. Chem.* **1988**, *27*, 191−197. (b) Jacobsen, H.; Kraatz, H.-B.; Ziegler, T.; Booran, P. M. *J. Am. Chem. Soc.* **1992**, *114*, 7851−7860. (c) Kraatz, H.-B.; Jacobsen, H.; Ziegler, T.; Boorman, P. M. *Organometallics* **1993**, *12*, 76−80. (d) McGuire, D. G.; Khan, M. A.; Ashby, M. T. *Inorg. Chem.* **2002**, *41*, 2202−2208.

and **10**, respectively, indicated that no interaction exists between Ni(II) and the thioether sulfur atom (Supplementary information).

Conclusion and Comments

Studies on the mononuclear Ni(II)−thiol complexes (**1**, **4**−**7**), Ni(III, II)−thiolate complexes (**2**, **3**), and Ni(II)−thioether complexes (**8a**, **8b**, **9**, **10**) have produced the following results.

(1) Neutral Ni^{II}−thiol complex **1** was synthesized and characterized by IR, ^1H NMR, UV−vis, and single-crystal X-ray diffraction. Complex **1** serves as a precursor for the syntheses of the anionic mononuclear Ni^{II}−thiol complexes **4**−**7** via a ligand-displacement reaction. On the basis of ^2H NMR and IR ν_{S-D} studies, the pendant thiol proton of complexes **1**/**4**−**7** is D_2O exchangeable.

(2) In complexes **1a**, **1b**, and **4**−**7**, the presence (strength) of the intramolecular [Ni−S···H−S] interaction (or a combination of intramolecular [Ni−S···H−S] and [Ni···H−S] interactions) was verified in the solid state by the observation of a lower IR ν_{S-H} stretching frequency compared to that of the free ligand P(*o*-$C_6H_4SH)_3$ (Table 1)[18] and was subsequently confirmed by a single-crystal X-ray diffraction. Single-crystal X-ray diffraction studies reveal that the Ni···S(1) distance falls into the range of 3.609−3.802 Å in Ni(II)−thiol complexes **1a** and **4**−**7** (type A), compared to those of 2.540 and 2.914 Å in the Ni(II)−thioether complexes **8a** and **8b** (type C). In contrast, the long Ni···S(1) distances (3.258 and 3.229 Å) found in complexes **9** and **10** indicated the absence of interaction between the Ni and S(1) atoms (type D). These results rule out the existence of an intramolecular Ni···S(1) interaction (Ni···S(1) distance of 3.609−3.802 Å) in complexes **1a**/**4**−**7** (type B) and may support the idea that the pendant thiol protons of Ni(II)−thiol complexes **1**/**4**−**7** were attracted by both nickel and the sulfur of thiolate, resulting in combinations of intramolecular [Ni−S···H−S] and [Ni···H−S] interactions (type A).

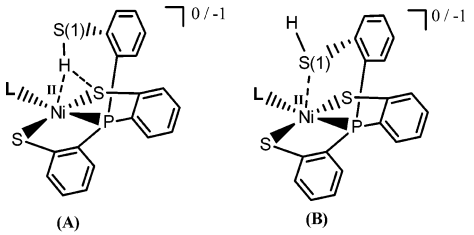

L = PPh_3 (**1**), SePh (**4**), Se-*p*-C_6H_4-Cl (**5**), Cl(**6**), 2-S-C_4H_3S (**7**)

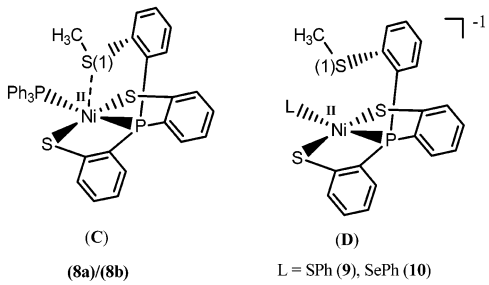

(3) The extent of the intramolecular [Ni−S···H−S] interaction (or a combination of intramolecular [Ni−S···H−S] and [Ni···H−S] interactions) was modulated by the distinct monodentate ligands PPh_3, [Se-*p*-C_6H_4-Cl]$^-$, [S-C_4H_3S]$^-$, [Cl]$^-$, and [SePh]$^-$ in complexes **1a** and **4**−**7**. The IR ν_{S-H} stretching frequency reflects that an increase in the Ni basicity (electronic density) regulated by the monodentate ligand arrests the proton of the pendant thiol effectively and causes the weaker S−H bond.

(4) Compared to the Ni···S(3) distances of 3.802 and 3.248 Å observed in complexes **1a** and **1b** (Scheme 1), the single-crystal X-ray structure revealed that thioether sulfur semi-bonding to Ni(II) (Ni···S(3) distance of 2.5397 Å) may exist in complex **8a** and that there is no interaction between Ni and S(3) (Ni···S(3) distance of 2.9135 Å) in complex **8b**. On the basis of the ^1H NMR spectra and single-crystal X-ray diffractions, the intramolecular interaction between Ni^{II} and the thioether sulfur atom became weaker when the temperature is increased or the more electron-donating monodentate ligand is ligated to the Ni^{II} center as observed in the mononuclear Ni^{II}−thioether complexes **8a**, **8b**, **9**, and **10**. Obviously, increasing the electron density on Ni should have the opposite effect on the interaction with RSH and RSR′. Increasing the electron density on Ni favors the interaction with S−H (Ni acts as a hydrogen-bond acceptor) and disfavors the interaction with S in SRS′ (RSR′ is an electron pair donor).

(5) Complexes **1** and **4**−**7** are sensitive toward O_2 to yield mononuclear Ni(III) thiolate complexes $[Ni^{III}(L)(P(o\text{-}C_6H_4S)_3)]^{0/1-}$ (L = PPh_3 (**2**), Se-*p*-C_6H_4−Cl (**11**), SePh (**12**), S−C_4H_3S (**13**)).[18] $[Ni^{II}(L')(P(o\text{-}C_6H_4S)_2(o\text{-}C_6H_4{-}SH))]^{0/1-}$ (L′ = Se-*p*-C_6H_4−Cl, SePh, S−C_4H_3S) and $[Ni^{II}(L')(P(o\text{-}C_6H_4S)_2(o\text{-}C_6H_4{-}SH))]^{0/1-}$, with the monodentate selenolate/thiolate ligands L′, show more O_2 sensitivity than complex **1**. It is presumed that the stronger intramolecular [Ni−S···H−S] interaction found in the $[Ni^{II}(L')(P(o\text{-}C_6H_4S)_2(o\text{-}C_6H_4{-}SH))]^{0/1-}$ complexes led to the weaker S−H bond strength and accelerated the oxidation of the $[Ni^{II}(L')(P(o\text{-}C_6H_4S)_2(o\text{-}C_6H_4{-}SH))]^{0/1-}$ complexes to produce complexes **11**−**13**.[18] A detailed study is underway. The isolation of complexes **1a** and **1b**−**10** may support the proposed proton-bonding type of the active site of the Ni-R and Ni-SI states in the catalytic cycle of [NiFe] hydrogenases.

Experimental Section

Manipulations, reactions, and transfers were conducted under nitrogen according to Schlenk techniques or in a glovebox (argon gas). Solvents were distilled under nitrogen from appropriate drying agents (diethyl ether from CaH_2; acetonitrile from $CaH_2-P_2O_5$; methylene chloride from CaH_2; hexane and tetrahydrofuran (THF) from sodium benzophenone) and stored in dried, N_2-filled flasks over 4 Å molecular sieves. Nitrogen was purged through these solvents before use. Solvent was transferred to the reaction vessel via stainless cannula under positive pressure of N_2. The reagents bis(triphenylphosphoranylidene)ammonium chloride ([PPN][Cl]) (Fluka), diphenyl diselenide, bis(4-chlorophenyl) diselenide, di(2-thienyl) disulfide, (triphenylphosphine) nickel(II) dichloride, and deuterium oxide, 99.9 atom % D (Aldrich) were used as received. Compound tris(2-thiophenyl)phosphine (P-(*o*-$C_6H_4SH)_3$) was syn-

thesized by published procedures.[19] Infrared spectra of the ν(SH) stretching frequencies were recorded on a Perkin Elmer model Spectrum One B spectrophotometer with sealed solution cells (0.1 mm, KBr windows) or KBr solid. UV−vis spectra were recorded on a GBC Cintra 10e. ^{1}H and ^{2}H NMR spectra were obtained on a Varian Unity-500 spectrometer. Electrochemical measurements were performed with a CHI model 421 potentionstat (CH Instrument). Cyclic voltammograms were obtained from a 2.0 mM analyte concentration in CH_2Cl_2 using 0.1 M [n-Bu_4N][PF_6] as a supporting electrolyte. Potentials were measured at 298 K versus a Ag/AgCl reference electrode using a glassy carbon working electrode. Under the conditions employed, the potential (V) of the ferrocinium/ferrocene couple was 0.39 (CH_2Cl_2). Analyses of carbon, hydrogen, and nitrogen were obtained with a CHN analyzer (Heraeus).

Preparation of [Ni^{II}(PPh$_3$)(P(*o*-C$_6$H$_4$S)$_2$(*o*-C$_6$H$_4$SH))] (1). $NiCl_2(PPh_3)_2$ (0.195 g, 0.3 mmol) and P(*o*-$C_6H_4SH)_3$ (0.108 g, 0.3 mmol) were dissolved in 5 mL of THF and stirred at ambient temperature for 20 min. Hexane (20 mL) was then added to precipitate the red solid [Ni^{II}(PPh$_3$)(P(*o*-C$_6$H$_4$S)$_2$(*o*-C$_6$H$_4$SH))] (**1**) (yield 0.160 g, 79%). Diffusion of hexane into the THF solution of complex **1** at room temperature for 5 days led to red-brown needle crystals identified by single-crystal X-ray diffraction as complex **1a**. In contrast, diffusion of hexane into the CH_2Cl_2 solution of complex **1** afforded dark red crystals characterized by single-crystal diffraction as complex **1b**. IR (KBr): complex **1a** 2393 (ν_{SH}) cm^{-1}; complex **1b** 2240 (ν_{SH}) cm^{-1}. ^{1}H NMR ($CDCl_3$): δ 5.908 (s) (SH), 6.992 (s), 7.180 (t), 7.297−7.421 (m), 7.708 (t). ^{31}P NMR ($CDCl_3$): δ 76.57 (d) ($J_{^{31}P-^{31}P}$ = 695 Hz, (P-(*o*-$C_6H_4S)_2$(*o*-C_6H_4SH)), 24.65 (d) ($J_{^{31}P-^{31}P}$ = 695 Hz, PPh_3) (vs H_3PO_4). Absorption spectrum (CH_2Cl_2) [λ_{max}, nm (ϵ, M^{-1} cm^{-1})]: 606 (181). Anal. Calcd for $C_{36}H_{28}P_2S_3Ni$: C, 63.83; H, 4.17. Found: C, 63.51; H, 3.73.

Preparation of [Ni^{III}(PPh$_3$)(P(*o*-C$_6$H$_4$S)$_3$)] (2). Dry oxygen gas (9 mL) was purged into a red THF solution (7 mL) of complex **1** (0.203 g, 0.3 mmol) at 0 °C. The reaction solution was stirred at 0 °C for an additional 30 min, and a significant change in color of the reaction solution from red to deep green was observed. Hexane (25 mL) was then added to precipitate the dark green solid [Ni^{III}(PPh$_3$)(P(*o*-C$_6$H$_4$S)$_3$)] (**2**) (yield 0.155 g, 76%). Diffusion of hexane into a CH_2Cl_2 solution of complex **2** at −15 °C for three weeks led to dark green crystals suitable for X-ray crystallography. ^{1}H NMR ($CDCl_3$): δ −3.99 (br), 5.48 (br), 8.42 (br), 9.70 (br), 11.82 (br), 12.62 (br), 13.67 (br). Absorption spectrum (CH_2Cl_2) [λ_{max}, nm (ϵ, M^{-1} cm^{-1})]: 611 (1777), 671 (1596), 1150 (1031). Anal. Calcd for $C_{36}H_{27}P_2S_3Ni$: C, 63.92; H, 4.02. Found: C, 63.71; H, 3.61.

Preparation of [PPN][Ni^{II}(PPh$_3$)(P(*o*-C$_6$H$_4$S)$_3$)] (3). Method A. [PPN][SPh] (0.323 g, 0.5 mmol) dissolved in CH_3CN (5 mL) was added to a stirred solution of complex **1** (0.339 g, 0.5 mmol) in THF (5 mL) under N_2 at ambient temperature. The reaction mixture was stirred for 3 h, and diethyl ether (25 mL) was added to precipitate the orange solid. The orange solid was dried under vacuum to give [PPN][Ni^{II}(PPh$_3$)(P(*o*-C$_6$H$_4$S)$_3$)] (**3**). Yield: 0.384 g, 63%.

Method B. A solution containing complex **2** (0.338 g, 0.5 mmol) and [PPN][SEt] (0.300 g, 0.5 mmol) in THF−CH_3CN (volume ratio 5:5 mL) was stirred at ambient temperature under N_2 for 3 h. Diethyl ether (25 mL) was then added to precipitate the orange solid. After the orange solid was dried under vacuum, complex **3** was isolated. Yield: 0.330 g, 54%. Red-orange crystals suitable for X-ray diffraction analysis were obtained by the diffusion of diethyl ether into a THF−CH_3CN (3:1 volume ratio) solution of complex **3** at 0 °C for one week. ^{1}H NMR (CD_3CN): δ 6.748 (t), 6.925 (t), 7.270−7.481 (m), 7.539−7.580 (m), 7.648 (t), 7.777 (t). Absorption spectrum (CH_2Cl_2) [λ_{max}, nm (ϵ, M^{-1} cm^{-1})]: 801 (533). $C_{72}H_{57}NP_4S_3Ni$: C, 71.17; H, 4.73; N, 1.15. Found: C, 70.54; H, 4.93; N, 1.64.

Protonation of Complex 3 by HClO$_4$. $HClO_4$ (28 μL, 0.2 mmol) was added dropwise to complex **3** (0.243 g, 0.2 mmol) in THF (5 mL) at 0 °C under a N_2 atmosphere. The reaction mixture was stirred for 30 min and then filtered through Celite to remove [PPN][ClO_4]. Hexane (10 mL) was added to precipitate the red solid, identified as complex **1** (0.076 g, 56%) by FTIR, UV−vis, and ^{1}H NMR spectra.

Reaction of Complex 3 and [Cp$_2$Fe][PF$_6$]. [Cp_2Fe][PF_6] (0.067 g, 0.2 mmol) dissolved in CH_3CN (5 mL) was added dropwise to the THF−CH_3CN (3:1 volume ratio) solution of complex **3** at 0 °C under a N_2 atmosphere. After the mixture was stirred for 30 min, it was dried under vacuum to produce a green-yellow solid, and then the green-yellow solid was redissolved in THF (5 mL). The THF solution was then filtered through Celite to remove [PPN][PF_6], and diethyl ether (20 mL) was added to precipitate the green solid. The green solid was washed twice with 20 mL diethyl ether and dried under vacuum to yield complex **2** (0.061 g, 45%) characterized by UV−vis and ^{1}H NMR spectra.

Reaction of Complex 1 and [PPN][SePh]/[PPN][Se-*p*-C$_6$H$_4$-Cl]. Complex **1** (0.067 g, 0.1 mmol) and [PPN][SePh] (0.069 g, 0.1 mmol) (or [PPN][Se-*p*-C_6H_4-Cl] (0.073 g, 0.1 mmol)) were dissolved in THF (4 mL) and stirred overnight under nitrogen at ambient temperature. Diethyl ether (10 mL) was then added to precipitate the red-brown solid, identified as [PPN][Ni^{II}(SePh)P-((*o*-C$_6$H$_4$S)$_2$(*o*-C$_6$H$_4$SH))] (**4**) (0.071 g, 61%) and [PPN][Ni^{II}(Se−C$_6$H$_4$-*p*-Cl)(P(*o*-C$_6$H$_4$S)$_2$(*o*-C$_6$H$_4$SH))] (**5**) (0.080 g, 70%) by FTIR, UV−vis, ^{1}H NMR spectra, and single-crystal X-ray diffraction.[18] Complex **5**. IR (KBr): 2283 (ν_{SH}) cm^{-1}. ^{1}H NMR (C_4H_8O): δ 8.39 (d) (S−H). Absorption spectrum (CH_2Cl_2) [λ_{max}, nm (ϵ, M^{-1} cm^{-1})]: 440 (4320). Anal. Calcd for $C_{58}H_{46}NP_3S_5Ni$: C, 65.17; H, 4.34; N, 1.31. Found: C, 65.04; H, 4.46; N, 1.01.

D/H Exchange for Reaction of Complexes 1/5 and D$_2$O. A 100-fold excess of D_2O (0.8 mL, 40 mmol) was added to a THF solution of complex **1** (THF−CH_3CN solution, 3:1 mL, volume ratio) or complex **5** (0.458 g, 0.4 mmol)) at 0 °C. The reaction solution containing complex **1** (or complex **5**) and D_2O was stirred for 30 min at 0 °C. Diethyl ether (3 mL) was then added to layer above the mixture. The flask was tightly sealed and kept in the refrigerator at −15 °C for one week. Red-brown crystals [Ni^{II}(PPh$_3$)-(P(*o*-C$_6$H$_4$S)$_2$(*o*-C$_6$H$_4$SD))] (**1-D**) were isolated. Yield: 0.155 g, 77%. IR (KBr): 1752 (ν_{SD}) cm^{-1}. ^{2}H NMR ($CDCl_3$): δ 6.175 (br) (SD) (using the natural abundance of D in C_4H_8O solvent, two singlet peaks at 1.73 and 3.57 ppm, as the internal standard). Red-brown crystals of [PPN][Ni(Se-*p*-C_6H_4−Cl)(P(*o*-$C_6H_4S)_2$(*o*-C_6H_4-SD))] (**5-D**) were isolated (0.398 g, 86.9%). IR (KBr): 1676 (ν_{SD}) cm^{-1}. ^{2}H NMR (CH_2Cl_2): δ 7.833 (br) (vs $CHDCl_2$, natural abundance of D in CH_2Cl_2 solvent, 5.32 ppm).

Preparation of [PPN][Ni^{II}Cl(P(*o*-C$_6$H$_4$S)$_2$(*o*-C$_6$H$_4$SH))] (6). Complex **1** (0.068 g, 0.1 mmol) and [PPN][Cl] (0.057 g, 0.1 mmol) were loaded into a 20 mL Schlenk tube. After THF (3 mL) was added to give a red solution, the solution mixture was stirred at ambient temperature overnight. Diethyl ether (12 mL) was then added to precipitate the red-brown solid, [PPN][Ni^{II}Cl(P(*o*-C$_6$H$_4$S)$_2$-(*o*-C$_6$H$_4$SH))] (**6**). Yield: 0.068 g, 69%. Red-brown crystals suitable for X-ray crystallography were obtained by the diffusion of diethyl ether into a THF−CH_3CN (3:1 volume ratio) solution of complex **6** at 0 °C for one week. IR (KBr): 2300 (ν_{SH}) cm^{-1}. ^{1}H NMR ($CDCl_3$): δ 5.808 (s) (SH), 6.818 (t), 6.905 (t), 7.025 (t), 7.188−7.298 (m), 7.403−7.488 (m), 7.637−7.666 (t). Absorption spectrum (CH_2Cl_2) [λ_{max}, nm (ϵ, M^{-1} cm^{-1})]: 605 (453), 876 (137). Anal.

Calcd for $C_{54}H_{43}P_3S_3ClNNi$: C, 65.57; H, 4.38; N, 1.42. Found: C, 64.80; H, 4.38; N, 1.19.

Preparation of [$Ni^{II}(PPh_3)(P(o\text{-}C_6H_4S)_2(o\text{-}C_6H_4\text{-}SCH_3))$] (8). A CH_3CN solution (3 mL) containing $[Me_3O][BF_4]$ (0.030 g, 0.2 mmol) was added dropwise to the THF−CH_3CN (3:1 volume ratio) solution of complex **3** at 0 °C under a N_2 atmosphere. After the mixture was stirred for 1 h, the volume of the reaction mixture was reduced under vacuum, and then methanol (10 mL) was added to precipitate the green solid. The green solid was washed twice with another 10 mL of methanol and dried under vacuum to produce green solid [$Ni^{II}(PPh_3)(P(o\text{-}C_6H_4S)_2(o\text{-}C_6H_4\text{−}SCH_3))$] (**8**). Yield: 0.162 g, 78%. Diffusion of hexane into a THF solution of complex **8** at 0 °C for three weeks led to dark green crystals characterized by X-ray crystallography as complex **8a**. However, diffusion of hexane into a THF solution of complex **8** at 30 °C for one week yielded dark green crystals (complex **8a**) and some red crystals which were characterized by single-crystal X-ray diffraction as complex **8b**. The X-ray diffraction analyses revealed the subtle differences between the red and green crystals. ^{1}H NMR (25 °C) ($CDCl_3$): δ 2.012 (s) (S−CH_3), 6.914 (t), 7.072 (t), 7.230−7.441 (m), 7.596−7.659 (m), 7.735−7.772 (m). VT ^{1}H NMR (C_4D_8O): δ 1.820 (−60 °C), ∼2.109 (60 °C) (s) (S-CH_3). Absorption spectrum (CH_2Cl_2) [λ_{max}, nm (ϵ, M^{-1} cm^{-1})]: 393 (3367), 609 (374). Anal. Calcd for $C_{37}H_{30}P_2S_3Ni$: C, 64.27; H, 4.37. Found: C, 64.56; H, 4.93.

Preparation of [PPN][Ni^{II}(L)($P(o\text{-}C_6H_4S)_2(o\text{-}C_6H_4\text{-}SCH_3)$)] (L = SPh (9), SePh (10)). Complex **8** (0.1 mmol, 0.069 g) and [PPN][SPh] (0.1 mmol, 0.065 g) (or [PPN][SePh], 0.1 mmol, 0.070 g) were loaded into a 20 mL Schlenk tube, and then 5 mL of THF was added to the tube via cannula under a positive pressure of nitrogen. After the reaction mixture was stirred overnight under N_2 at room temperature, the green solution completely converted into a red-brown solution. Hexane (10 mL) was then added to precipitate the red-brown solid. The red-brown solid was washed twice with 10 mL of diethyl ether and dried under vacuum to afford [PPN][Ni^{II}(SPh)($P(o\text{-}C_6H_4S)_2(o\text{-}C_6H_4\text{-}SCH_3)$)] (**9**) (0.074 g, 68%) (or [PPN][Ni^{II}(SePh)($P(o\text{-}C_6H_4S)_2(o\text{-}C_6H_4\text{-}SCH_3)$)] (**10**), 0.088 g, 78%). Suitable red crystals of complexes **9** and **10** for single-crystal X-ray diffraction were obtained by diffusion of diethyl ether into the THF solution of complexes **9** and **10**, respectively. Complex **9**. ^{1}H NMR ($CDCl_3$): δ 2.553 (s) (SCH_3), 6.684 (t), 6.750 (t), 6.862−6.904 (m), 6.990 (t), 7.194−7.454 (m), 7.587−7.619 (m), 7.708−7.725 (m). Absorption spectrum (CH_2Cl_2) [λ_{max}, nm (ϵ, M^{-1} cm^{-1})]: 445 (2015). Anal. Calcd for $C_{61}H_{50}NP_3S_4Ni$: C, 68.03; H, 4.68; N, 1.30. Found: C, 68.03; H, 4.44; N, 1.29. Complex **10**. ^{1}H NMR ($CDCl_3$): δ 2.528 (s) (SCH_3), 6.684 (t), 6.843−6.900 (m), 6.992 (t), 7.182−7.453 (m), 7.584−7.616 (m), 7.837−7.856 (m). Absorption spectrum (CH_2Cl_2) [λ_{max}, nm (ϵ, M^{-1} cm^{-1})]: 478 (1816). Anal. Calcd for $C_{61}H_{50}NNiP_3S_3Se$: C, 65.19; H, 4.48; N, 1.25. Found: C, 64.55; H, 5.02; N, 0.95.

Magnetic Measurements. The magnetization data were recorded on a SQUID magnetometer (MPMS5 Quantum Design company) with an external 1 T magnetic field for complex **2** in the temperature range of 2−300 K. The magnetic susceptibility of the experimental data was corrected for diamagnetism by the tabulated Pascal's constants.

Crystallography. The crystals chosen for the X-ray diffraction studies measured 0.40 × 0.35 × 0.20 mm for complex **1a**, 0.40 × 0.30 × 0.30 mm for complex **1b**, 0.25 × 0.20 × 0.10 mm for complex **2**, 0.32 × 0.20 × 0.20 mm for complex **3**, 0.50 × 0.45× 0.40 mm for complex **5**, 0.20 × 0.15 × 0.15 mm for complex **6**, 0.35 × 0.33 × 0.15 mm for complex **8a**, 0.30 × 0.15 × 0.15 mm for complex **8b**, 0.4 × 0.32 × 0.27 mm for complex **9**, and 0.30 × 0.25 × 0.25 mm for complex **10**. Each crystal was mounted on a glass fiber and quickly coated in epoxy resin. Unit-cell parameters were obtained by least-squares refinement. Diffraction measurements for complexes **1a**, **1b**, **2**, **3**, **5**, **6**, **8a**, **8b**, **9**, and **10** were carried out on a SMART CCD (Nonius Kappa CCD) diffractometer with graphite-monochromated Mo Kα radiation (λ = 0.7107 Å) between 2.07 and 27.50° for complex **1a**, 1.45 and 27.50° for complex **1b**, 1.35 and 27.50° for complex **2**, 1.33 and 27.50° for complex **3**, 1.24 and 27.50° for complex **5**, 1.26 and 27.50° for complex **6**, 1.25 and 27.50° for complex **8a**, 1.48 and 27.50° for complex **8b**, 1.23 and 27.50° for complex **9**, and 1.23 and 28.31° for complex **10**. Least-squares refinement of the positional and anisotropic thermal parameters of all non-hydrogen atoms and fixed hydrogen atoms (H(3A) in complex **1** and H(2S) in complex **6**) was based on F^2. A SADABS absorption correction was made.[21] The SHELXTL structure refinement program was employed.[22]

Acknowledgment. We gratefully acknowledge financial support from the National Science Council (Taiwan).

Supporting Information Available: X-ray crystallographic files in CIF format for the structure determinations of [$Ni^{II}(PPh_3)(P\text{-}(o\text{-}C_6H_4S)_2(o\text{-}C_6H_4SH))$], [$Ni^{III}(PPh_3)(P(o\text{-}C_6H_4S)_3)$], [PPN][$Ni^{II}(PPh_3)(P(o\text{-}C_6H_4S)_3)$], [PPN][Ni(Se-*p*-$C_6H_4$-Cl)($P(o\text{-}C_6H_4S)_2(o\text{-}C_6H_4SH)$)], [PPN][Ni(Cl)$P((o\text{-}C_6H_4S)_2(o\text{-}C_6H_4SH))$], [$Ni^{II}(PPh_3)(P(o\text{-}C_6H_4S)_2(o\text{-}C_6H_4\text{−}SCH_3))$], [PPN][$Ni^{II}$(SPh)($P(o\text{-}C_6H_4S)_2(o\text{-}C_6H_4\text{-}SCH_3)$)], and [PPN][$Ni^{II}$(SePh)($P(o\text{-}C_6H_4S)_2(o\text{-}C_6H_4\text{-}SCH_3)$)] and figures showing ^{1}H NMR spectra of **8** and an ORTEP drawing of **10**. This material is available free of charge via the Internet at http://pubs.acs.org.

IC051924W

(21) Sheldrick, G. M. *SADABS, Siemens Area Detector Absorption Correction Program*; University of Göttingen: Göttingen, Germany, 1996.
(22) Sheldrick, G. M. *SHELXTL, Program for Crystal Structure Determination;* Siemens Analytical X-ray Instruments Inc.: Madison, WI, 1994.